Spectrogram-based synchrosqueezing transform and its second-order version

Gang Yu
School of Electrical Engineering
University of Jinan
Jinan, China
yugang2010@163.com

Abstract—**This paper focuses on the issue how to obtain the concentrated result for a time-varying signal. Recently, the synchrosqueezing transform (SST) has drawn considerable attentions, which can highly enhance the concentration of the conventional methods. In the paper, we prove that, when the window is selected as Gaussian function, the spectrogram can also be used for deriving the SST technique. In which, for the weakly time-varying signal and the strongly time-varying signal, we derive the first-order SST and the second-order SST, respectively. We also use the real-world signal for validating the effectiveness of this methods.**

Keywords Time-frequency analysis; synchrosqueezing transform; time-varying signal processing.

I. INTRODUCTION

In practical engineering, the signals recorded by the sensors, such as vibration, sound and pressure often tend to be time-varying. Time-frequency (TF) analysis (TFA) method has been accepted as one of the most effective tools for dealing with such signals [1]. The conventional TFA methods such as short time Fourier transform (STFT) have to suffer from heavily blurry energy problem, which cannot provide the precise results for the practical signals. In signal processing fields, the recently proposed synchrosqueezing transform (SST) has drawn considerable attentions, which can highly improve the concentration of the conventional methods [2-6]. Meanwhile, the SST method is invertible, which can be used for mode decomposition or signal de-noising. In mathematics, a time-varying signal can be expressed as

$$s(t) = A(t)e^{i\varphi(t)} \tag{1}$$

where the A(t) and $\varphi(t)$ are the amplitude and phase, and $\varphi'(t)$ denotes the instantaneous frequency (IF). For such a signal, the STFT can be expressed as

$$G(t,\omega) = \int_{-\infty}^{+\infty} s(u)e^{-i\omega(u-t)}g(u-t)du. \tag{2}$$

However, STFT result usually smears heavily, since the window function *g(t)* cannot compactly support both in the TF domain simultaneously. To improve this situation, the SST method is proposed as

$$Ts(t,\eta) = \int_{-\infty}^{+\infty} \delta(\eta - \hat{\omega}(t,\omega))G(t,\omega)d\omega \tag{3}$$

With the aid of the SST technique, we can highly enhance the concentration of the STFT. In Eq. (3), the most important procedure is to calculate the parameter $\hat{\omega}(t,\omega)$, which makes sure that $\hat{\omega}(t,\omega) = \varphi'(t)$. For the original SST technique, this parameter is often calculated from the TF coefficients. In this letter, we will show that, when the *g(t)* is selected as the Gaussian function, the parameter $\hat{\omega}(t,\omega)$ can also be calculated from spectrogram, i.e. $|G(t,\omega)|$, which can be instructive to propose more effective SST techniques.

II. SPECTROGRAM-BASED SYNCHROSQUEEZING TRANSFORM

To derive the spectrogram-based SST, it needs that the considered signal should be weakly time-varying. Therefore, we can expand the amplitude and phase of the considered signal *s(u)* at the time instant *t* by zero-order and first-order Taylor expansion, i.e.

$$s(u) = A(t)e^{i(\varphi(t)+\varphi'(t)(u-t))}. \tag{4}$$

Substituting Eq. (4) into Eq. (2), we can deduce,

$$G(t,\omega) = A(t)e^{i\varphi(t)}\hat{g}(\omega-\varphi'(t)) \tag{5}$$

where $\hat{g}()$ is Fourier transform of the g(*t*). Considering that the $\hat{g}()$ supports in the frequency domain, for the signal (4), the energy of the STFT result should smear around the signal IF. Herein, we let the window be

$$g(t) = e^{-(2\beta)^{-1}t^2}. \tag{6}$$

We can derive the STFT spectrogram,

$$P(t,\omega) = |G(t,\omega)| = A(t)\sqrt{2\pi\beta}e^{-\frac{\beta(\omega-\varphi'(t))^2}{2}}. \tag{7}$$

Then, calculating the derivative of the spectrogram to have

978-1-7281-0860-5/19/$31.00 ©2019 IEEE

$$\partial_\omega P(t,\omega) = A(t)\sqrt{2\pi\beta}e^{-\frac{\beta(\omega-\varphi'(t))^2}{2}}(-\beta(\omega-\varphi'(t))). \quad (8)$$

Moreover, calculating the parameter $\hat{\omega}(t,\omega)$ to have

$$\hat{\omega}(t,\omega)=\omega+\frac{\partial_\omega P(t,\omega)}{\beta P(t,\omega)}. \quad (9)$$

According to Eq. (8) and Eq. (9), it is easy to derive $\hat{\omega}(t,\omega)=\varphi'(t)$. Substituting Eq. (9) into Eq. (3), it can derive that,

$$\begin{aligned} Ts(t,\eta)&=2\pi\int_{-\infty}^{+\infty} g(u-t)s(u)\delta(u-t)du\cdot\delta(\eta-\varphi'(t)) \\ &=2\pi A(t)e^{i\varphi(t)}\delta(\eta-\varphi'(t)). \end{aligned} \quad (10)$$

The Eq. (10) denotes that, compared with the STFT result, the concentration of the SST result is highly enhanced, since the Dirac delta function is zero everywhere except at zero. However, for the Eq. (10), it only holds when the considered signal is weakly time-varying. It also means that the Eq. (10) is the first-order SST. Furthermore, we will derive that, when the signal is strongly time-varying, the spectrogram can also be used for generating a high-resolution TF result. For a strong time-varying signal, we should expand the instantaneous phase with second-order Taylor expansion, i.e.,

$$s(u) = A(t)e^{i(\varphi(t)+\varphi'(t)(u-t)+0.5\varphi''(t)(u-t)^2)}. \quad (11)$$

Substituting Eq. (11) into Eq. (2), the spectrogram can be derived that,

$$P(t,\omega) = \left|G(t,\omega)\right| = A(t)\sqrt{\frac{2\beta\pi}{1+\beta^2\varphi''(t)^2}}e^{-\frac{\beta(\omega-\varphi'(t))^2}{2+2\beta^2\varphi''(t)^2}}. \quad (12)$$

Substituting Eq. (12) into Eq. (9) to have the parameter $\hat{\omega}(t,\omega)$ that,

$$\hat{\omega}(t,\omega)=\omega-\frac{\omega-\varphi'(t)}{1+\beta^2\varphi''(t)^2}. \quad (13)$$

Furthermore, we have,

$$\left|\hat{\omega}(t,\omega)-\varphi'(t)\right| = \left|\frac{\beta^2\varphi''(t)^2}{1+\beta^2\varphi''(t)^2}(\omega-\varphi'(t))\right|. \quad (14)$$

The Eq. (14) denotes that, for a more complex signal, the (9) is no more suitable for estimating the precise parameter. According to Eq. (13), we can have,

$$\varphi'(t) = \left(\hat{\omega}(t,\omega)-\omega\frac{\beta^2\varphi''(t)^2}{1+\beta^2\varphi''(t)^2}\right)(1+\beta^2\varphi''(t)^2). \quad (15)$$

Inspired by Eq. (15), calculating the derivative of $\hat{\omega}(t,\omega)$ respectively, i.e.

$$\partial_t\hat{\omega}(t,\omega) = \frac{\varphi''(t)}{1+\beta^2\varphi''(t)^2}. \quad (16)$$

$$\partial_\omega\hat{\omega}(t,\omega) = \frac{\beta^2\varphi''(t)^2}{1+\beta^2\varphi''(t)^2}. \quad (17)$$

Then, according to Eq. (15), we can further derive that,

$$\varphi'(t) = \left(\frac{\partial_\omega\hat{\omega}(t,\omega)}{(\partial_t\hat{\omega}(t,\omega))^2}\right)\left(\hat{\omega}(t,\omega)-\omega\partial_\omega\hat{\omega}(t,\omega)\right). \quad (18)$$

Therefore, we can define a novel parameter $\hat{\omega}^{[2]}(t,\omega)$ that is expressed as

$$\hat{\omega}^{[2]}(t,\omega) = \left(\frac{\partial_\omega\hat{\omega}(t,\omega)}{(\partial_t\hat{\omega}(t,\omega))^2}\right)\left(\hat{\omega}(t,\omega)-\omega\partial_\omega\hat{\omega}(t,\omega)\right). \quad (19)$$

According to Eq. (18), having $\hat{\omega}^{[2]}(t,\omega)=\varphi'(t)$. For (3), we replace the $\hat{\omega}(t,\omega)$ with $\hat{\omega}^{[2]}(t,\omega)$, it is easy to obtain that,

$$Ts(t,\eta) = 2\pi A(t)e^{i\varphi(t)}\delta(\eta-\varphi'(t)). \quad (20)$$

The Eq. (20) illustrates that, for the signal (11), it can also provide a concentrated TF result. Considering that the Eq. (20) is established on the strongly time-varying signal, hence it is called second-order SST. Therefore, it can be concluded that, when the window g(t) is Gaussian function, we can also derive the SST technique and its second-order version based on the spectrogram. Then, we consider the reconstruction ability of the proposed SST methods. We first calculate the integral of the SST representation with respect to frequency variable,

$$\int_{-\infty}^{+\infty} Ts(t,\eta)d\eta = (2\pi g(0))s(t) \quad (21)$$

where N = 1 or 2. It is obvious that the signal allowing the following reconstruction,

$$s(t) = (2\pi g(0))^{-1}\int_{-\infty}^{+\infty} Ts(t,\eta)d\eta. \quad (22)$$

III. NUMERICAL ANALYSIS

We construct a multi-component signal, which consists a weakly time-varying signal S1 and a strongly time-varying signal S2. This signal is modelled as Eq. (23). The TF result of the first-order SST method is displayed in Fig. 1. We plot the local TF features of two components in a short time in Fig. 1(c-d). It can be seen that, in this short time, the IF of the signal S1 has a slower change than the signal S2, and the TF energy of the S1 is more concentrated than that of the S2. It demonstrates that the first-order SST technique only provides a satisfactory TF representation for weakly time-varying signal. In Fig. 2, the TF representation of the second-order SST is displayed. It can be observed that, the TF features of both of two signals are highly concentrated. It means that the second-order SST has the better capacity for dealing with strongly time-varying signals than first-order SST.

$$S(t) = \underbrace{\sin(2\pi(40t+\sin(1.5t)))}_{S1} + \underbrace{\sin(2\pi(17t+6\sin(1.5t)))}_{S2} \quad (23)$$

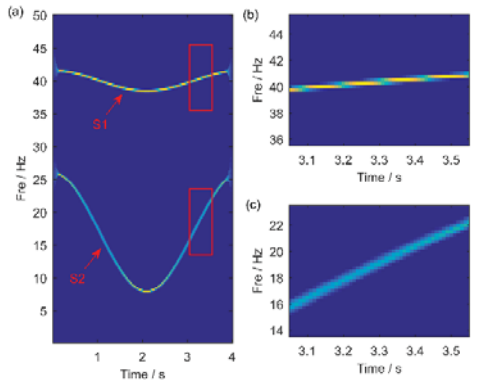

Fig. 1 (a) The first-order SST result, the zoomed versions on (b) signal S1 and (c) signal S2.

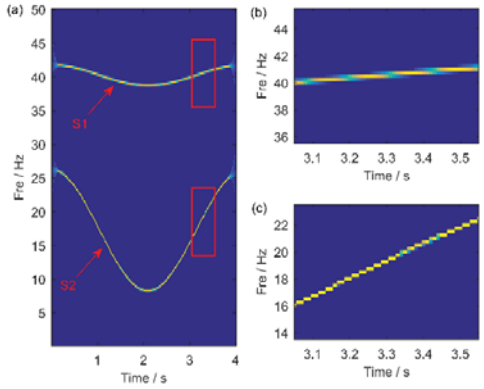

Fig. 2 (a) The second-order SST result, the zoomed versions on (b) signal S1 and (c) signal S2.

IV. REAL-WORLD EXPERIMENT ANALYSIS

An abnormal vibration of a rotating machinery [2-6] is analyzed. The structure is shown in Fig. 3. The rotating machinery is supported by two bearings which is driven by a motor. The screws in positions P1, P2, P3 and P4 are loosen to produce the misalignment fault. The displacement sensor is to record the vibration signal of the shaft. Meanwhile, the instantaneous speed of the shaft is also recorded. The shaft speed firstly increases about from 900 rpm to 1600 rpm, then decreases to 800 rpm.

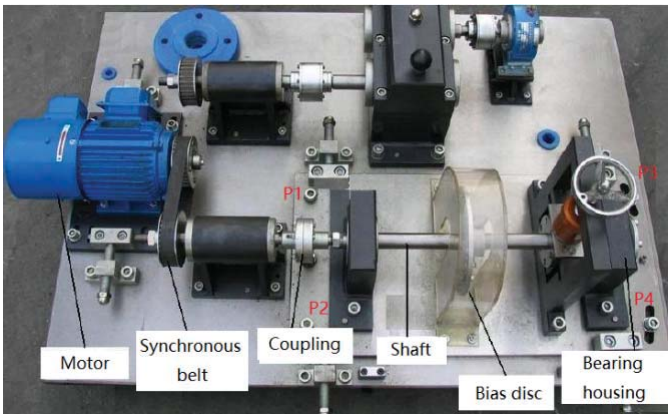

Fig. 3. The structure of the test rig.

The shaft speed is first plotted in Fig. 4(a). The signal and the corresponding frequency spectrum are plotted in Fig. 4(b-c). It is shown that the main frequency component concentrates on the frequency band of 20-30 Hz. Other than this, we cannot obtain any useful information about the fault of the machinery. The TF results of first-order SST and second-order SST are displayed in Fig. 5. It is obviously observed that, the first-order component (C1) and its high-order components (C2 and C3) are characterized by the first-order SST. Moreover, the second-order SST significantly enhances the energy concentration of the TF result. All components are characterized with highly concentrated energy. In which, the component C1 has the largest TF energy, which is also consistent with the shaft speed. Thus, it can be known that, the misalignment fault signal of the rotating machinery consists of the basic component and the high-order components. The basic component should have the highest energy and is determined by the shaft speed. Therefore, we can diagnose the misalignment fault of the rotating machinery according to this TF feature.

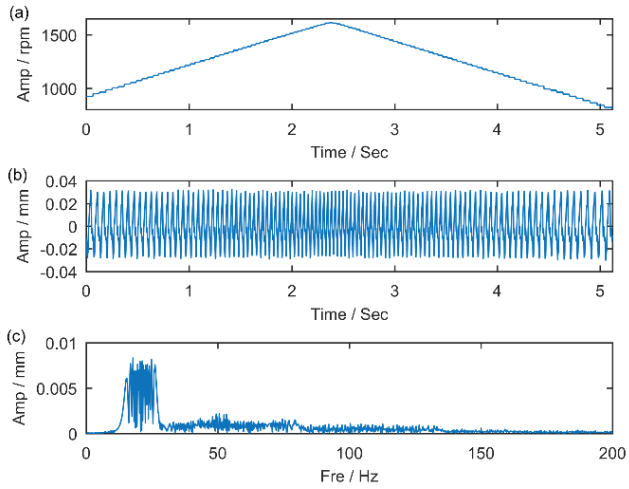

Fig.4. (a) The instantaneous speed of the shaft, (b) vibration signal and (c) the spectrum.

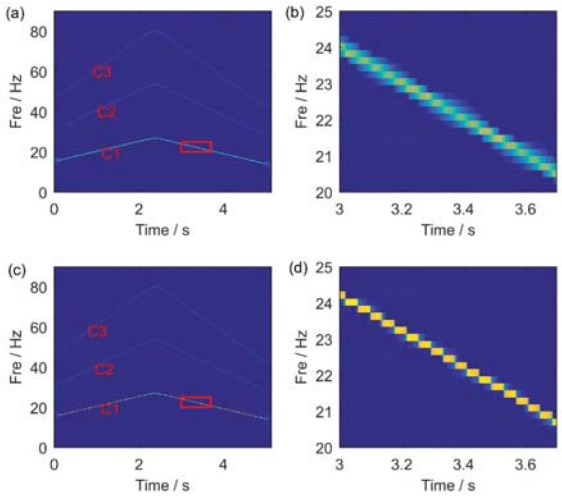

Fig. 5 (a) First-order SST result, (b) zoomed version, (c) second-order SST result and (d) zoomed version.

V. CONCLUSION

In this paper, we have shown that, when the window *g(t)* of STFT is Gaussian function, the SST method and its second-order version can be derived from the spectrogram, which is an inspiring supplement for the SST techniques. In which, the second-order SST has better capacity for dealing with more complex signals. Moreover, both of two proposed SST methods is of reversibility, which can be used for mode decomposition or signal de-noising.

REFERENCES

[1] Daubechies I, Lu J, Wu H T. Synchrosqueezed wavelet transforms: An empirical mode decomposition-like tool. Applied and computational harmonic analysis, 2011, 30(2): 243-261.

[2] Yang Y, Zhang W, Peng Z, et al. Multicomponent signal analysis based on polynomial chirplet transform. IEEE Transactions on Industrial Electronics, 2013, 60(9): 3948-3956.

[3] Yu G, Yu M, Xu C. Synchroextracting transform. IEEE Transactions on Industrial Electronics, 2017, 64(10): 8042-8054.

[4] Yu G, Wang Z, Zhao P. Multisynchrosqueezing Transform. IEEE Transactions on Industrial Electronics, 2019, 66(7): 5441-5455.

[5] Chen S, Du M, Peng Z, et al. High-accuracy fault feature extraction for rolling bearings under time-varying speed conditions using an iterative envelope-tracking filter. Journal of Sound and Vibration, 2019, 448: 211-229.

[6] Shi J, Liang M, Necsulescu D S, et al. Generalized stepwise demodulation transform and synchrosqueezing for time–frequency analysis and bearing fault diagnosis. Journal of Sound and Vibration, 2016, 368: 202-222.